Electronic Supplementary Material (ESI) for Journal of Materials Chemistry

Spin crossover materials evaporated in clean high vacuum and ultra-high vacuum conditions: from thin films to single molecules

Tatiana Palamarciuc, Jenny C. Oberg, Fadi El Hallak, Cyrus F. Hirjibehedin, Michele Serri, Sandrine Heutz, Jean-François Létard and Patrick Rosa

Contents

Sublimation under primary vacuum

For both compounds **1** and **2**, prior to using the HV facilities we checked sublimation in standard laboratory conditions using an ice-cold finger under primary vacuum (≈ 0.1mbar), that is in similar conditions to those used by Naggert *et al.* in their previous work.[1] After complete sublimation (2-3 days at 120°C for compound **1** and 130°C for compound **2**), the pale violet condensates were scratched from the glass and analysed chemically and physically (see further down). Powder materials from both processes A and B yielded some brown residue leftover in the crucible. Elemental analysis of this residue showed no surviving compound (CHNS, diffuse reflectance measurements) in this brown residue. A similar brown residue was observed later on during sublimation in UHV with high temperatures. This brown residue is likely to be due to some decomposition process, as observed previously for $[Fe(phen)_2(NCS)_2]$.[2] We found that this residue was not formed if we evaporated single crystals in UHV conditions and at temperatures below 80 °C.

Physical characterization details

Elemental analyses

Elemental analyses were performed by the Pregl-Dumas method on a ThermoFischer Flash EA1112 (C, H, N) and by ICP-OES on an Varion 720-ES (B, Fe).

X-ray diffraction

Powder X-ray diffraction data were recorded using a PANalytical X'Pert MPD diffractomer with Bragg-Brentano geometry, Cu Kα radiation (λ = 1.54056 Å) and a backscattering graphite 370 monochromator, using either standard Al sample holders or low background Si wafers. Single crystals cell parameters were measured at room temperature on a Bruker-Nonius κ-CCD diffractometer, using graphite monochromated Mo-Kα radiation (λ = 0.71073 Å). X-Ray Diffraction on thin films were recorded with a Panalytical X-pert Powder diffractometer, with Bragg-Brentano geometry, Cu Kα radiation and a nickel filter to remove Kβ radiation, using low background Si wafers as sample holders. The measurements were performed at room temperature.

Raman spectroscopy

Raman spectra were recorded using a Renishaw Raman microscope, at an excitation wavelength of 785 nm. All measurements were taken at room temperature and the Raman Shift was measured from 100 cm^{-1} to 1800 cm^{-1}.

Variable temperature reflectance spectroscopy

Reflectance was investigated by using a home-built set-up coupled with a SM240 spectrometer (Opton Laser International), which allows both the reflectance spectrum to be collected in the range of λ=450-950 nm at a given temperature and the temperature dependence of the signal at a selected wavelength (± 2.5 nm) between 5 and 290 K to be followed. Samples were irradiated with light over the entire temperature range. The diffuse reflected signal was calibrated by activated charcoal (Merck) as a black standard and barium sulfate ($BaSO_4$, DIN50533, Merck) as a white standard. The instrument is also equipped with an optical detector, which collects the entire reflected intensity and gives the total reflectivity signal as a function of temperature. Analyses were performed on thin layers of the samples without any dispersion in a matrix.

Magnetic and photomagnetic measurements

Magnetic measurements were performed with MPMS-7 and MPMS-5 Quantum Design SQUID magnetometers. Bulk measurements were performed over the temperature range 10-250 K using the RSO probe under a 1 T field, on powder samples sealed in 30 µm-thick polyethylene bags and accurately weighed with a Mettler MX5 microbalance. Thin films (90x3 mm strips) on Kapton sheets (10x10 cm) were rolled as tight cylinders and inserted in SQUID straws. Photomagnetic measurements were performed by using a Spectrum Physics Series 2025 Ar^+/Kr^+ laser (λ = 532 or 676 nm) coupled by means of an optical fiber to the cavity of the SQUID magnetometer, the power at the sample surface being adjusted at 5 $mW.cm^{-2}$, with the DC probe under a 5 T field. Small squares (≈3x3 mm) of Cu tape or Kapton sheet supporting the thin films were placed on top of a sample holder made of a drinking straw cut in half, with one half covered with some wrapping polyethylene film, then both

[1] H. Naggert, A. Bannwarth, S. Chemnitz, T. von Hofe, E. Quandt and F. Tuczek, *Dalton Trans.*, **2011**, *40*, 6364.

[2] M. Bernien, *X-Ray Absorption Spectroscopy of Fe Complexes on Surfaces: Electronic Interactions and Tailoring of the Magnetic Coupling*, Ph. D. Thesis, Freie Universität Berlin, Germany, **2009**.

ends were inserted in the SQUID straw. Samples were slowly cooled to 10 K to avoid thermal trapping of HS species, then irradiated and the change in magnetic moment monitored. Upon saturation light was switched off and magnetic moment measured with temperature increased at a rate of 0.3 $K.min^{-1}$ to determine the T(LIESST) value. Strips and squares macroscopic dimensions were carefully measured with a juniper and/or an optical microscope, then the corresponding calculated volume was divided by the reported room-temperature crystal volume cell and multiplied by the 4 molecules per cell to yield the molarity of the samples. Data treatment used thicknesses as measured by the quartz crystal balance adjusted to fit bulk high temperature values : 355 nm for compound **1** was corrected to 296 nm, and 564 nm for compound **2** was corrected to 404 nm.

Raw data were treated to correct for spurious scans, centring drift and sample size and inhomogeneities. A magnetic multipolar model was used,[3, 4] using a multipole expansion described previously.[5, 6] A standard Levenberg-Marquardt least-squares fit, based on the 7th order multipole expansion described by equation (15) of ref 6, yields the total magnetic moment[7] as the dipolar contribution (the only one directly proportionate to the volume magnetization, see ref 5). We found empirically this method to be much less sensitive to sample shape, centring errors and sample holder off-centre contributions, especially so when measuring very small signals. It is applied in the Cryogenics SQUID system.[8] For the bulk measurements, resulting magnetic moments were corrected for polyethylene diamagnetic contributions: with m the mass of the polyethylene bag, T the temperature in K and H the magnetic field in Oe, to the moment in emu was substracted

$$\left(-8.07e^{-7} + {1.73e^{-9}}/{T}\right) mH$$

For "strip" films measurements, resulting magnetic moments were considered as originating purely from the sample due to the sample disposition adopted. For photomagnetic measurements, Cu or Kapton substrates contributions were approximated by considering the thin film as diamagnetic in the dark below the spin crossover temperature. Those contributions were then substracted from magnetic moments after irradiation. All data was then corrected for sample diamagnetic contributions approximated by the Pascal constants ($-255e^{-6}$ $cm^3.mol^{-1}$ for complex **1**, $-265e^{-6}$ $cm^3.mol^{-1}$ for complex **2**).

Scanning tunnelling and atomic force microscopy

Scanning tunneling microscopy was performed using an Oxford Instruments STM with a flow cryostat for operation at liquid helium temperatures. Atomic force microscopy measurements were performed with a Veeco Dimension 3100 at room temperature operated in the tapping mode.

[3] J. Clarke, A. I. Braginski (Eds.) *The SQUID Handbook vol. II Applications of SQUIDs and SQUID Systems*, **2004**, Wiley-VCH.
[4] P. Stamenov, J. M. D. Coey, *Rev. Sci. Instr.*, **2006**, *77*, 015106.
[5] U. Ausserlechner, P. Kasperkovitz, W. Steiner, *Meas. Sci. Technol.*, **1994**, *5*, 213.
[6] U. Ausserlechner, P. Kasperkovitz, W. Steiner, *Meas. Sci. Technol.*, **1998**, *9*, 989.
[7] Quantum Design, MPMS Application Note 1014-213, 2002.
[8] http://www.cryogenic.co.uk/products/measurement/s600x.asp

Table S1 : Elemental analyses results for complexes 1 and 2

Elemental analyses of all products show that in both cases only the single-crystals after being carefully washed with cold water once give truly clean products. Processes A and B give good results, except process A for compound **2**. Nevertheless carbon content is systematically too low ; in our experience this is usually symptomatic of some contamination by another species.

Complex **1**, $C_{22}H_{24}B_2FeN_{10}$, 505.96 g/mol

	C	H	N	B	Fe
calculated	52.22	4.78	27.68	4.27	11.04
Process A	51.63	4.66	27.27	4.82	11.43
Process A after sublimation	51.63	4.87	26.94	4.27	11.04
Process B	51.30	4.77	27.36	4.76	11.84
Process B, handpicked single crystals	51.72	4.99	27.29	*	*
Process B, single crystals after washing	52.23	4.92	27.97	3.79	11.13

Complex **2**, $C_{24}H_{24}B_2FeN_{10}$, 529.98 g/mol

	C	H	N	B	Fe
calculated	54.39	4.56	26.43	4.08	10.54
Process A	48.91	4.40	30.05	*	*
Process B	53.76	4.65	26.38	*	*
Process B handpicked single crystals	48.56	4.49	20.32	*	*
Process B, single crystals after washing	54.36	4.69	26.69	3.77	10.86

* Not determined after CHN measurement

Figure S2 : X-ray powder diffractograms for compound 1 and 2

X-ray powder diffractograms for both processes and after sublimation show that compounds **1** and **2** can be obtained as well crystallized phases identical to the reported room temperature crystal structure, with crystallinity preserved upon sublimation. No difference is seen between processes A and B for compound **1**; for compound **2**, diffractograms show a mixture of phases for process A, preserved upon sublimation, agreeing with the unsatisfactory elemental analysis.

No background correction (air and sample holder diffusion, electronic noise, low-angle noise due to slit opening) was performed, thus the normalization process used yields an increased vertical offset respective to the starting diffractograms. Some 2θ offset may also be observed due to height misalignement of the sample with the sample holder. Spin crossover compounds can't be crushed without altering their properties, so sample holders were simply filled and excess sample removed with a glass plate applied lightly.

Complex 1: powder patterns for powders obtained through process A (black curve), after sublimation of this powder (red curve) and through process B (green curve), compared to the pattern calculated from atomic positions available in the Cambridge Structural Database (reference NEFTEX01, blue curve). For comparison all curves were normalized relative to the (11-1) reflection at 10.18°.

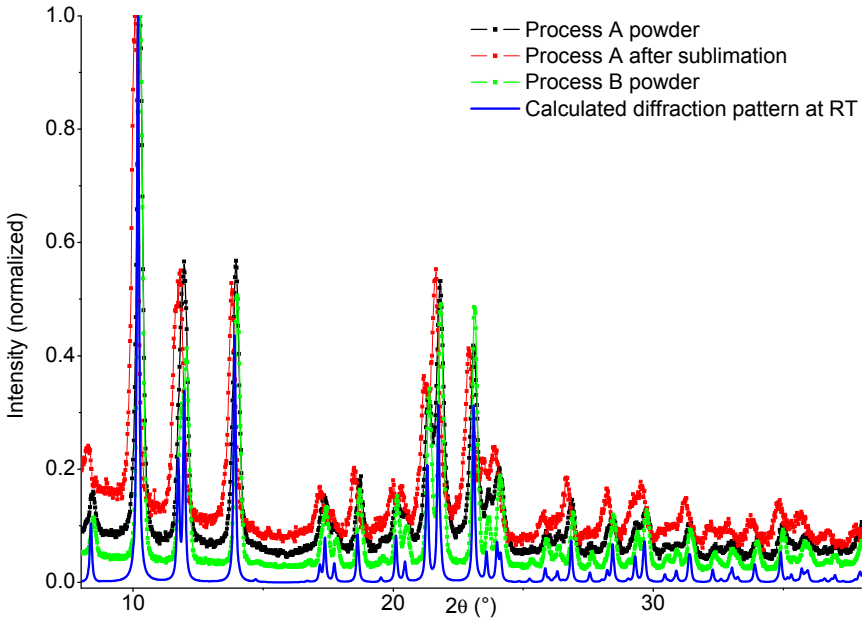

Complex 2: powder patterns for powders obtained through process A (black curve), after sublimation of this powder (red curve) and through process B (green curve), compared to the pattern calculated from atomic positions available in the Cambridge Structural Database (reference NEFSUM, blue curve). For comparison all curves were normalized relative to the (11-1) reflection at 10.01°. The impurity diffraction pattern is partly evidenced with black stars.

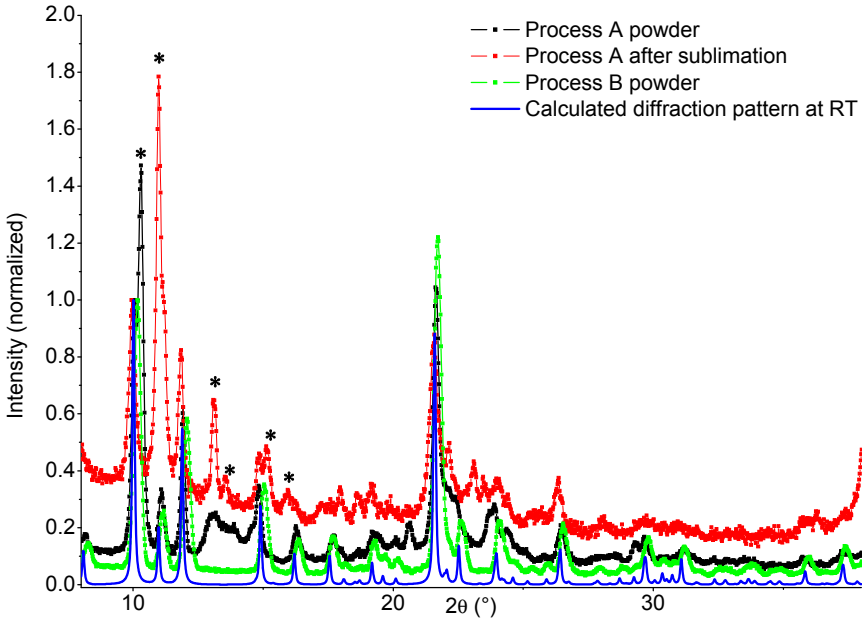

Variable temperature optical characterization of compounds 1 and 2

For both compounds, below 650 nm diffuse absorbance is close to unity due to the Metal-to-Ligand Charge Transfer (MLCT) band responsible for the deep-violet colour of the compounds. Evolution of the absorbance about 830 nm, where the d-d transition of the HS state lies, shows the characteristic decrease associated with the expected thermal SCO and the increase at lower temperatures associated with photoinduced SCO. Temperatures associated with thermal and photoinduced SCOs, viz. 155(5) K and 59(2) K respectively for compound **1** (Figure **S3**), and 160(5) K and 52(3) K (Figure **S4**) respectively for compound **2**, are in line with those reported in earlier works for thermal SCO[9] and photoinduced SCO.[10] The somewhat higher values given by reflectance spectroscopy are accounted for the fact that measurements are performed under constant illumination, while T(LIESST) measurements are performed in the dark after photoconversion. For compound **2**, Light-Induced Thermal Hysteresis (LITH)[11] is observed at low temperatures, as expected[12] for a strongly cooperative compound such as **2** when cooled under constant irradiation.

Figure S3 : variable temperature optical spectra of compound 1

Diffuse absorbance spectra for compound obtained through process B: powder (left) and single crystals (right).

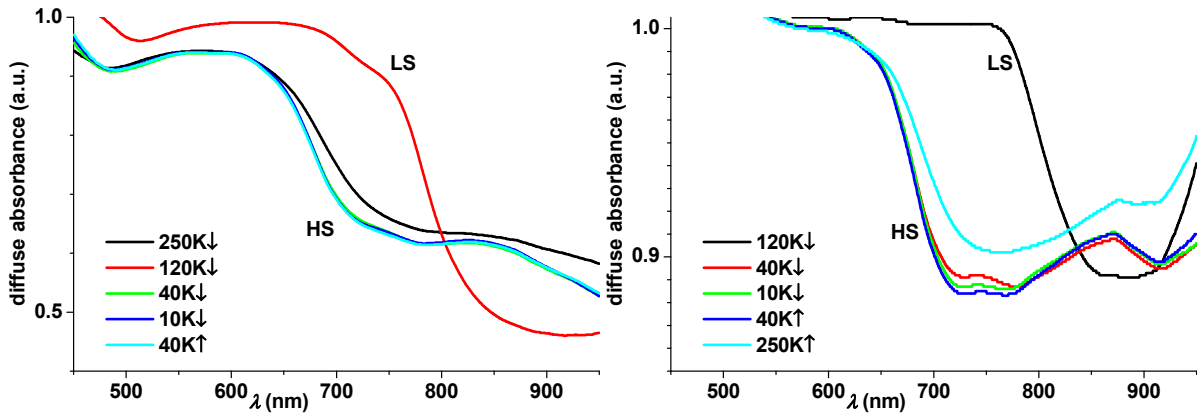

Diffuse absorbance at 647 nm and 830 nm for powders obtained through process A, before and after sublimation, and through process B (left) and for single crystals obtained through process B (right).

[9] J. A. Real, M. C. Muñoz, J. Faus and X. Solans, *Inorg. Chem.*, **1997**, *36*, 3008.
[10] N. Moliner, L. Salmon, L. Capes, M. C. Muñoz, J.-F. Létard, A. Bousseksou, J.-P. Tuchagues, J. J. McGarvey, A. C. Dennis, M. Castro, R. Burriel and J. A. Real, *J. Phys. Chem. B*, **2002**, *106*, 4276.
[11] J.-F. Létard, P. Guionneau, L. Rabardel, J.A.K. Howard, A.E. Goeta, D. Chasseau, O. Kahn, *Inorg. Chem.* **1998**, *37,* 4432.
[12] a) A. Desaix, O. Roubeau, J. Jeftic, J. G. Haasnoot, K. Boukhedadden, E. Codjovi, J. Linares, M. Nogues, F. Varret *Eur. Phys. J. B.* **1998**, *6*, 183; b) C. Enachescu, H. Constant-Machado, E. Codjovi, J. Linares, K. Boukheddaden, F. Varret *J. Phys. Chem. Solids*, **2001**, *62*, 1409.

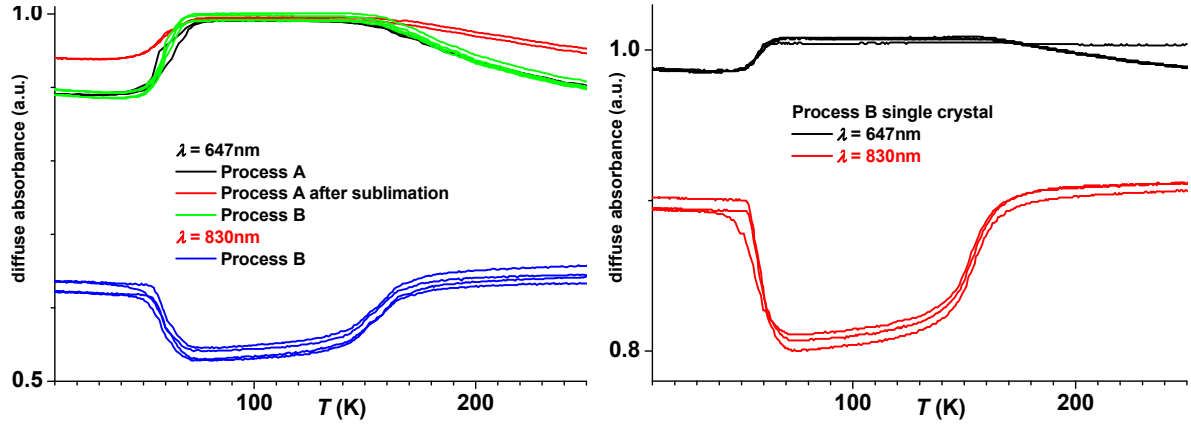

Note that since optical thickness is not measured, the diffuse absorbance scale is relative to the black (charcoal) and white (barium sulphate) calibration standards used. An absorbance close to 1 means that the measured compound reflects as little light as charcoal.

Figure S4 : variable temperature optical spectra for compound 2

Diffuse absorbance spectra for compound obtained through process B.

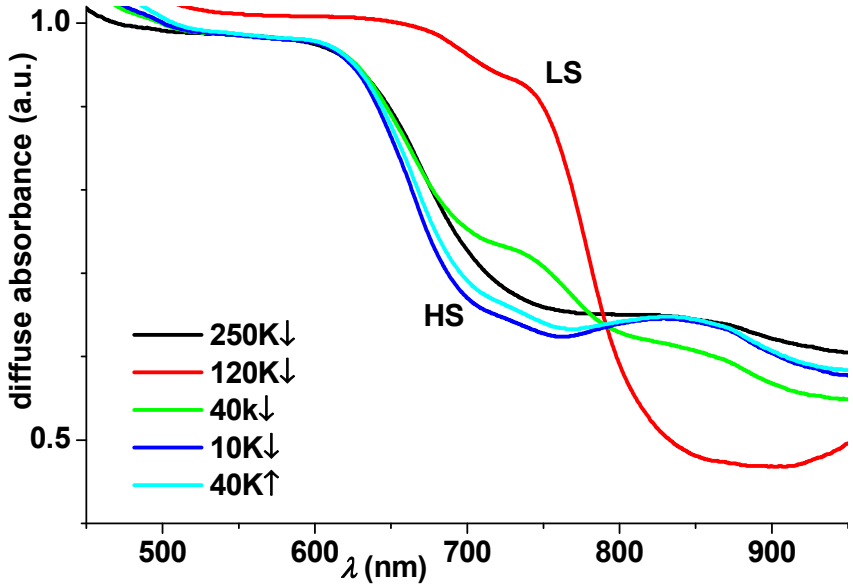

Diffuse absorbance at 647 nm and 830 nm for powders obtained through process A, before and after sublimation, and through process B.

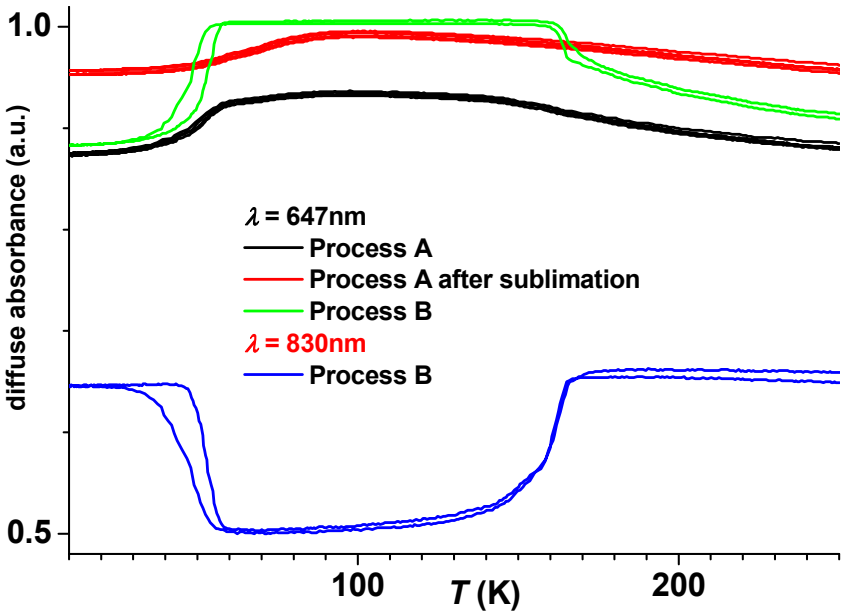

Figure S5 : AFM image of compound 1 evaporated on Gold

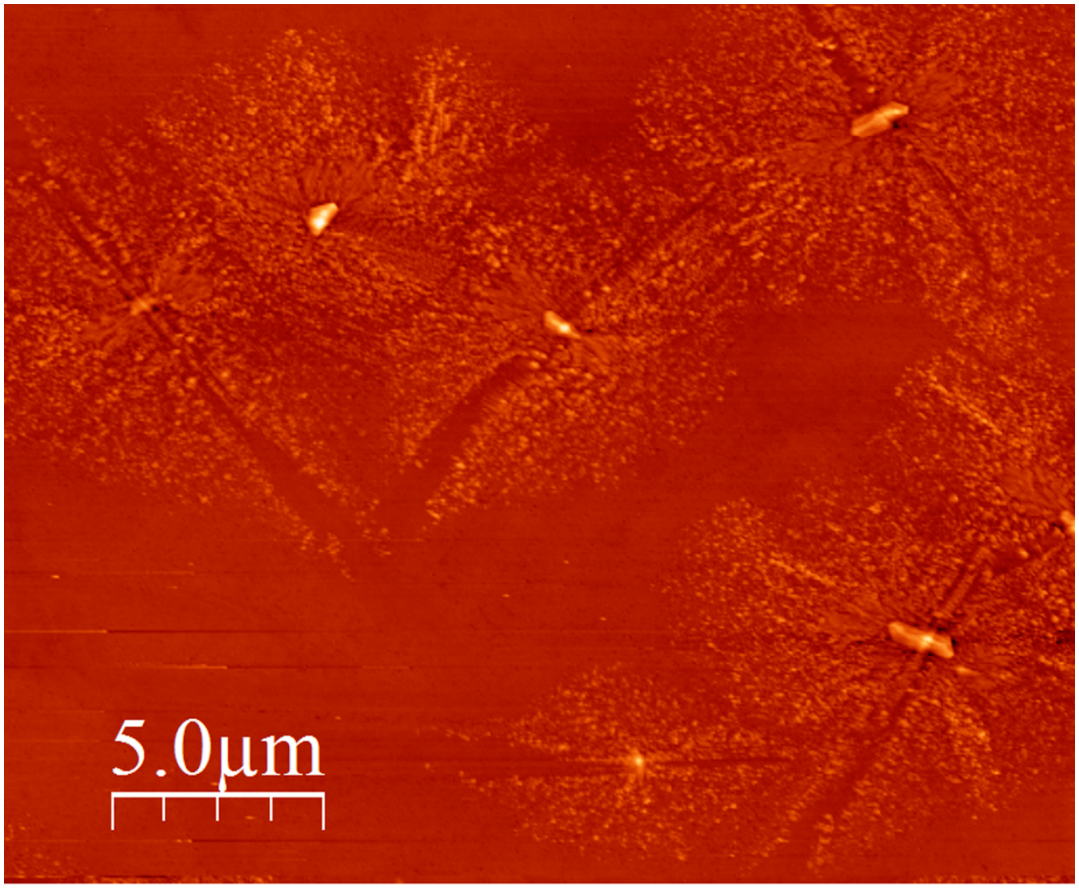

Figure S6 : AFM image of compound 2 evaporated on Gold

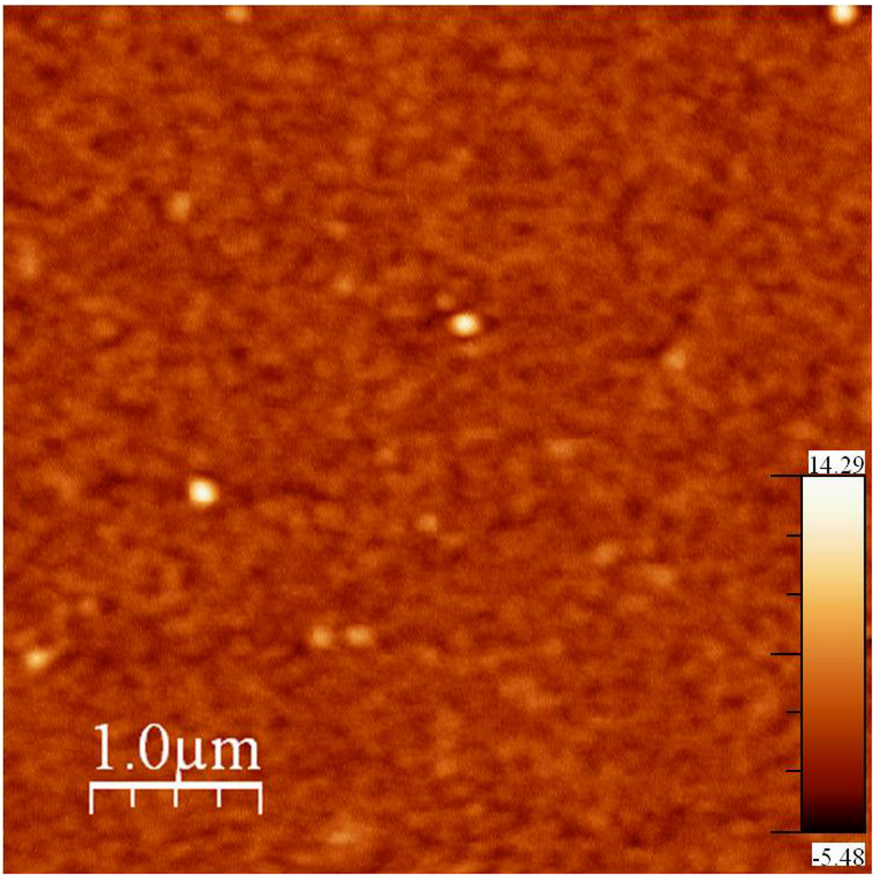

Figure S7 : Raman spectra of compound 1

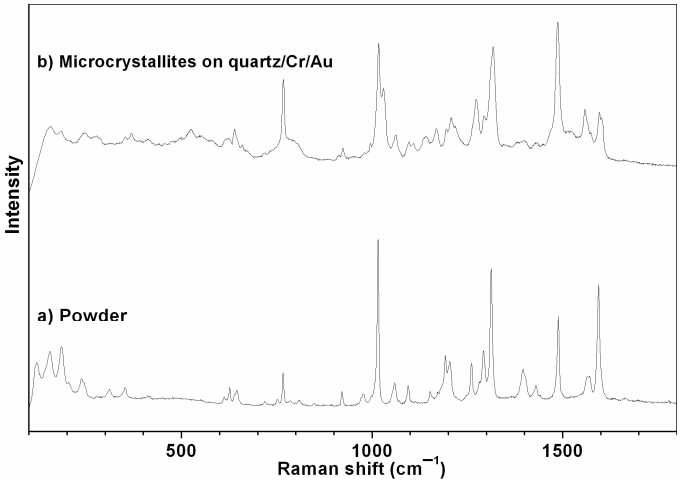

Comparing the features found (cm^{-1}). Overal agreement is evidenced in bold.

Compound **1** Powder	Compound **1** thin film microcrystallites
120	
154	***155***
185	***185***
204	
237	***239***
311	
	277
351	***351***
612	***612***
626	***626***
645	***645***
718	
752	
767	***767***
785	
810	***811***
848	
921	***921***
978	
1015	***1017***
1059	***1061***
1094	***1095***
1152	
1171	
1192	***1195***
1204	***1207***
1261	
	1271
1291	***1293***
1312	***1315***
1396	***1396***
1429	***1429***
1488	***1489***
1567	
1594	***1595***

Figure S8 : Raman spectra of compound 2

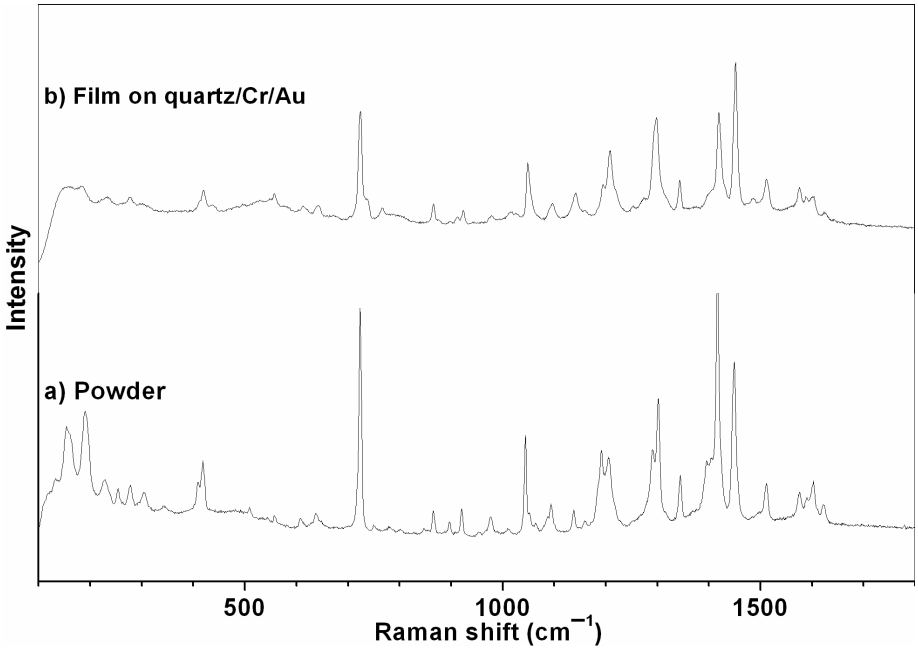

Comparing the features found with shifts for the HS state at 300 K.[10] Overal agreement is evidenced in bold.

Compound 2 Powder	Compound 2 Film	Litterature
133		136
154	156	
189	***185***	***189***
229	***231***	***231***
254		253
		258
278	***278***	***277***
305		308
343		
409		410
418		418
508		503
569	557	
		589
607	***613***	***607***
638	***642***	***638***
		703
723	723	724
	766	
865	***865***	***865***
897	***897***	***899***
920	***923***	***920***
977	***978***	***977***
1009		
	1016	
1043	***1048***	***1044***
1094	***1094***	***1095***
1137	***1140***	***1137***
1159	1160	

1192	***1195***	***1193***
1204	***1207***	***1207***
1294	***1296***	***1292***
1302		1303
		1317
1344	***1346***	***1346***
1396		1398
1417	***1418***	***1419***
1449	***1450***	***1451***
1512	***1512***	***1514***
1576	***1576***	***1578***
1602	***1602***	***1605***
1622	***1622***	***1626***

Figure S9 : X-ray diffraction of compound 1 thin film on Cu and glass

X-ray diffraction of the microcrystalline film of compound **1** on Cu (top), showing diffraction from planes (11-1) and (200), and on glass (bottom), showing diffraction from planes (11-1), (200) and (111). Corresponding 2θ angles calculated using indexation from the room temperature structure (reference NEFTEX01 in the Cambridge Structural Database) are 10.18°, 11.96° and 13.91° respectively. No other peaks were observed at higher angles.

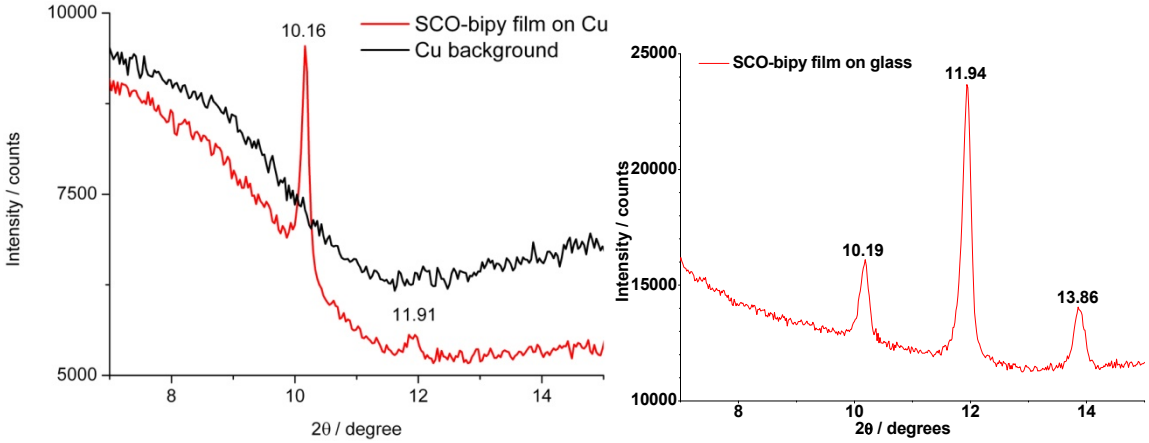

The significantly increased diffraction of the (200) plane for the film deposited on glass respective to the bulk strongly support a preferential (200) orientation. When considering the room temperature crystal structure (NEFTEX01), compound **1** molecules form columns along c, as shown in the representation below. Those columns are formed through π-stacking of the pyridine rings between molecules (distance between centroids of the pyridine rings is 3.8896(8)Å). The preferential (200) orientation as observed on glass is thus quite natural.

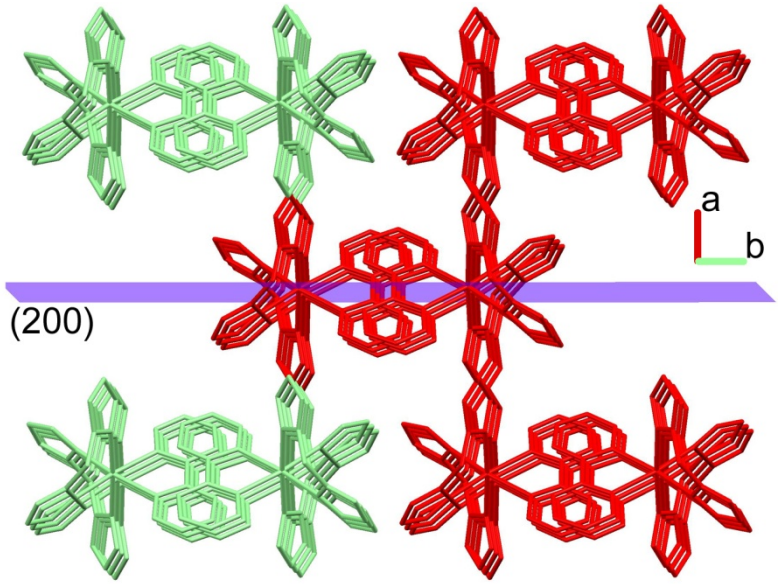

Representation of NEFTEX01 crystal packing as seen along c. Columns are represented in red or green for clarity. The (200) plane is represented in violet.

The (11-1) Bragg peak is the most intense one in the bulk powder diffractogram and is expected to be the one most easily seen, so a possible preferential orientation of the film on Cu is not a clear-cut case. Nevertheless, when looking at the NEFTEX01 crystal packing, a preferential (11-1) orientation on the

substrate would have the bipyridine ligands lying at about 45° to the surface, pointing alternatively towards and away from the substrate (see figure below, molecules in green and red respectively). It can be seen that in the green configuration, one pyridine ring and one {BH_2(pyrazole)} fragment are available to bind to the surface. The red configuration can then stack along c through the pyridine rings (the π-stacking is represented in hashed violet).

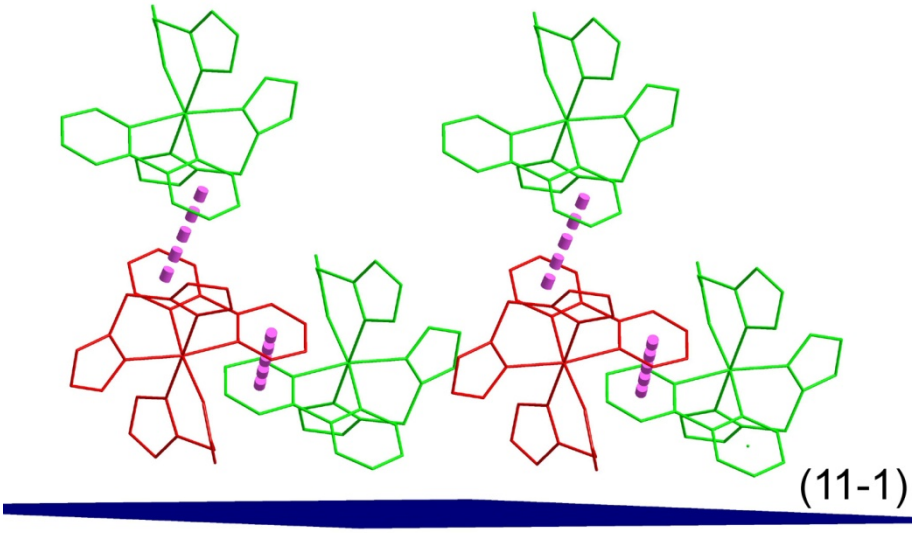

Representation of NEFTEX01 crystal packing as seen along [1-10]. Molecules with bipyridine pointing towards the substrate are represented in green, away from the substrate in red. The (11-1) plane is represented in blue.

Figure S10 : X-ray diffraction of compound 2 thin film on Cu and glass

X-ray diffraction of the microcrystalline film of compound **2** on Cu showing diffraction from plane (020) close to the $2\theta = 10.98°$ value found using indexation from reference NEFSUM in the Cambridge Structural Database. No other peaks were observed at higher angles, and no peaks at all were observed for compound **2** on glass.

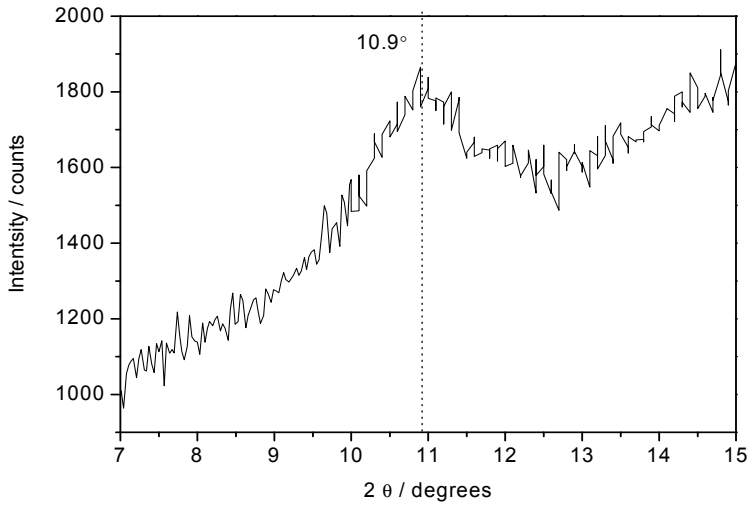

In the room temperature crystal structure (NEFSUM), compound **2** molecules form columns along *c*. Those columns are formed through weak π-stacking of the phenantroline rings between molecules (distance between centroids of the rings is 4.2499(7)Å).The figure below represent those columns as seen along *c*, with the (020) plane represented in violet. Molecules of compound **2** may be oriented with the phenantroline normal to the substrate pointing towards (in red) or away from it (in green).

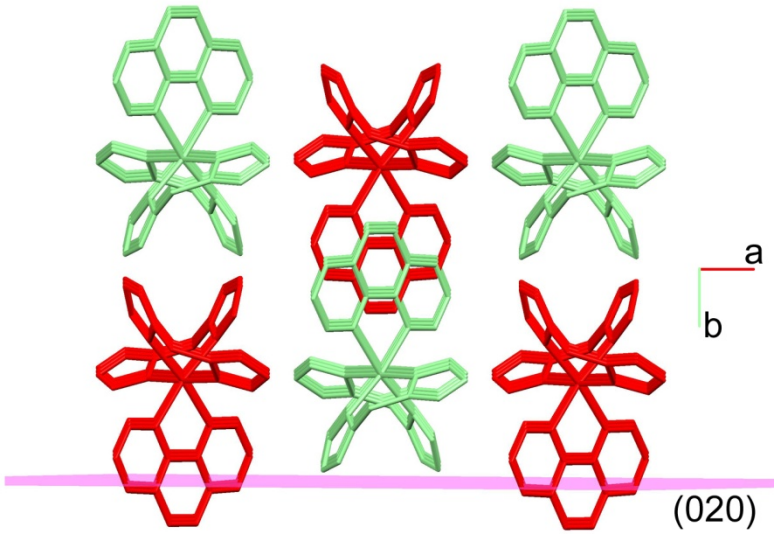

Representation of NEFSUM crystal packing as seen along c. Molecules with phenantroline pointing towards the substrate are represented in red, away from the substrate in gree. The (020) plane is represented in violet.

Figure S11 : Magnetic monitoring of compound 1 and 2 thin films upon irradiation

Baseline contributions were substracted from the measured magnetic moments. Lines are solely drawn as guide to the eye. Irradiation was performed at 676 nm, power at the sample was about 5 mW.cm^{-2}.